Original Article

Adaptive model predictive control of a six-rotor electric vertical take-off and landing urban air mobility aircraft subject to motor failure during hovering

**Shen Qu[1], Guoming Zhu[1] $\textcolor{green}{\circledR}$, Weihua Su[2], Sean Shan-Min Swei[3],
Mariko Hashimoto[4] and Tao Zeng[5]**

Abstract

In this article, motor failure control of a six-rotor electric vertical take-off and landing (eVTOL) urban air mobility aircraft is investigated using adaptive model predictive control (MPC) based on the linear parameter-varying (LPV) model developed using the nonlinear rigid-body aircraft model. For capturing the aircraft dynamics under motor failure conditions, a family of linearized models are obtained by trimming the nonlinear aircraft model at multiple equilibrium conditions and the LPV model is obtained by linking the linear models using the failed rotor speed, where the system transition from healthy to failure is modeled by a scheduling parameter calculated based on failed rotor speed caused by available motor peak power after failure. The proposed adaptive MPC is developed to optimize the system output performance, including the rigid-body aircraft velocity and altitude, by using quadratic programming optimization with reference compensation subject to a set of time-varying constraints representing the current available propeller acceleration calculated based on the motor power. Simulation study is conducted based on the developed LPV control design and original nonlinear rigid-body model, and the simulation results demonstrate that the designed adaptive MPC controller is able to recover and maintain the aircraft at desired stable condition after motor failure.

Introduction

Urban air mobility (UAM) has attracted tremendous attention from the vehicle industry and academia community. It is viewed as the promising future as part of next-generation transportation and expected to be a quiet, fast, clean, efficient, and safe point-to-point transportation. Since the complete concept of UAM is still under exploration, a consensus has not yet been achieved completely within the community. Researchers are following their design philosophy and guidelines in UAM vehicle development. One of the most promising and popular UAM concepts is electric vertical take-off and landing (eVTOL) vehicles. Equipped with distributed electric propulsion system, eVTOL vehicles use multiple electric motors and propellers to provide the lift force for vertical take-off and landing, which has been adopted by many leading eVTOL companies, for example, Boeing Aurora, Airbus A3, Joby Aviation, and Lilium. At the same time, eVTOL-related areas are widely investigated, including market prediction,[1] voyage planning,[2–5] power and energy modeling and optimization,[6–11] dynamics analysis,[12] and failure study.[13] Compared with a traditional helicopter, an eVTOL vehicle has not only enhanced diversification of power distribution, including position

and tilting freedom, but also fast-response electric motors. Therefore, the eVTOL vehicle dynamics is complicated and challenging to control, especially under motor failure condition.

Hovering control has always been crucial for vehicle safety consideration, especially when the aircraft is under motor failure situation, and many control strategies were exploited to recover from it. Traditional proportional-integral-derivative (PID) control is developed in Ref. 14 for crash-resistant purpose. Also, fault tolerant control strategy is applied to an octocoptor[15] using a super twisting sliding mode observer in the case of single motor failure. In Ref. 16, linear quadratic regulator is used for a morphing quadrotor vehicle, assuming that one motor

---

[1] Michigan State University, East Lansing, MI, USA
[2] The University of Alabama, Tuscaloosa, AL, USA
[3] Khalifa University, Abu Dhabi, UAE
[4] DENSO CORPORATION, Kariya, Japan
[5] DENSO International America, Inc., Southfield, MI, USA

Corresponding author:
Guoming Zhu, Department of Mechanical Engineering, Michigan State University, 1497 Engineering Research Court, Room E148, East Lansing, MI 48824, USA.
Email: zhug@egr.msu.edu

output torque goes to zero instantly. However, the control input constraints (e.g., maximum propeller driven torques) are not considered in this case, which is not practical since the feasibility of control solution will affect the closed-loop system performance, especially under motor failure condition.

The model predictive control (MPC) theory becomes a good candidate for the UAM hovering control due to its capability of handling a set of constraints.[17–19] For eVOTL aircraft hovering control, motor power is one of the most crucial constraints to be considered. Also, comparing with traditional PID control that requires a huge amount of tuning effort to make it work, MPC uses a specific set of design weightings to shape the target performance. Note that in order to make the MPC real-time implementable, a linear time-invariant (LTI) system model is often used for MPC control design. Often, a linearized model at current hovering condition can be obtained and used for MPC design, but it is difficult to obtain an LTI model during the transition from normal hovering to motor failure condition. With the development of adaptive MPC[20,21] and LPVmodeling method,[22–24] the adaptive MPC strategy–designed based on the LPV system model has been widely used for parameter-varying systems, which is aimed to improve closed-loop system performance.[25, 26]

In this article, based on a nonlinear six-rotor eVTOL UAM aircraft model, developed using formulation synthesizing complicated dynamics in Ref. 27, an LPV control design model is developed based on a set of LTI models obtained by linearizing the nonlinear one under different failed rotor speeds and an adaptive MPC strategy is developed based on the developed LPV control design model with time-varying control (motor torque) constraints calculated based on the available power of motors driving propellers under failure condition. For improving the closed-loop system performance and reducing the real-time computational cost, a set of feedback dynamic reference compensation equations is developed and calibrated. The simulation investigation is conducted by applying the designed adaptive MPC strategy to both LPV and nonlinear rigid-body UAM models in Matlab/Simulink environment.

The main contribution of the article is threefold. First, an LPV control design model is developed based on a set of LTI models obtained by linearizing the nonlinear rigid-body model under different failed rotor speeds. Second, an adaptive MPC design framework with control input constraints and dynamic reference compensation is proposed for studying recovery control with hovering motor failure, and last, the adaptive MPC strategy is validated using the nonlinear eVTOL model under motor failure situations.

The article is organized as follows. The section LPV Modeling Under Motor Failure reviews the nonlinear rigid-body model for the eVTOL UAM aircraft, followed by the LPV system model under varying equilibrium conditions. The section Adaptive MPC Controller Design of LPV System provides detailed discussions of the adaptive MPC design, followed by simulation studies in the section Simulation Results and Discussions. Last, the Conclusion adds conclusions and future work.

LPV modeling under motor failure

System modeling

In this section, the aircraft dynamics under multiple failure conditions are modeled as an LPV system obtained based on the original nonlinear aircraft model[27] considering aircraft rigid-body dynamics, inertial and gyroscopic loads, and longitudinal aerodynamics as well as rotor kinematics and thrusts. Figure 1 shows the modeled aircraft geometry with six rotors at 90° orientation (fuselage not shown), and Table 1 lists the model inertial parameters of rigid-body and fixed-wing aircraft as well as its rotors. Assuming that the aircraft is hovering at a fixed altitude with a varying propeller speed due to partial motor failure, the six-rotor torque (acceleration) levels are used as control input, denoted as u_1 to u_6. As for system outputs, besides the six degree of freedom rigid-body linear and angular displacements and speeds, the six propeller speeds are also used as outputs.

First, a set of LTI state-space models are obtained by linearizing (trimming) the nonlinear rigid-body model at each motor failure condition. For this study, the front-right motor (# 1 in Figure 1) is selected as the failed one with available peak power at 100% (normal), 66%, and 33% of the power under normal hovering condition, and the six propeller speeds are listed in Table 2. The mid-left motor (#4 in Figure 1) failure is also studied.

The obtained LTI system matrices are formulated as $A \in \mathbb{R}^{18 \times 18}$ and $B \in \mathbb{R}^{18 \times 6}$ defined in Table 3. The aircraft body coordinates are defined as y, z, and x; see Figure 2.

The system output matrix C is an 18-dimensional identity matrix, assuming all system states are measurable. The system inputs, states, and outputs are defined in Table 3. Finally, the discrete-time LTI system models are in the form of equation (1), where i presents the LTI model index and $i = 1, 2, 3$ denoting models at 100%, 66%, and 33% available motor power, respectively

$$\begin{cases} \Delta x(k+1) = A_i \Delta x(k) + B_i \Delta u(k) \\ \quad \Delta y(k) = C \Delta x(k) \end{cases} \quad (1)$$

Affine LPV system with equilibrium condition variation

With the set of LTI models obtained by trimming the nonlinear model at different equilibrium conditions, a direct method to obtain control design LTI model is selecting the corresponding LTI model near the current operational condition. However, to improve the model accuracy, a LPV modeling method is introduced.[28] where an LPV
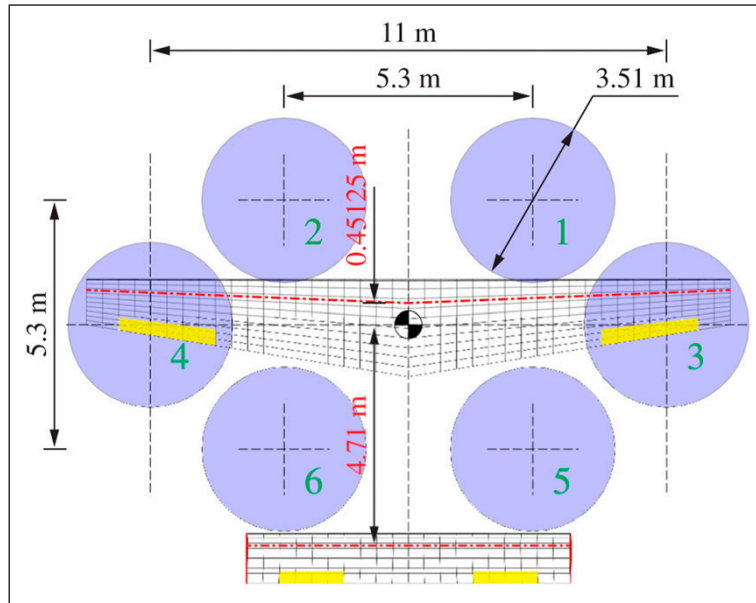
Figure 1. Geometry of urban air mobility aircraft (top view).

Table 1. Inertial properties of urban air mobility aircraft.

Body mass (kg)	Body moment of inertia (kg)			Rotor mass (kg)	Rotor moment of inertia (kg)		
m_B	$I_{B,xx}$	$I_{B,yy}$	$I_{B,zz}$	m_r	$I^e_{r,xx}$	$I^e_{r,yy}$	$I^e_{r,zz}$
2240.7276	12,000	9400	20,000	4.5454	3.5	7.0	3.5

Table 2. Equilibrium conditions of hovering under rotor #1 failure.

Model index	1	2	3
Available front-right motor power (% of normal hovering)	100%	66%	33%
Front right speed (rad/s)	100.7	87.7	69.6
Front left speed (rad/s)	100.7	106.7	113.2
Mid right speed (rad/s)	100.7	106.7	113.2
Mid left speed (rad/s)	100.7	106.7	113.2
Rear right speed (rad/s)	100.7	106.7	113.2
Rear left speed (rad/s)	100.7	87.7	69.6

model is a linear state-space model (see below) with coefficient matrices as an affine function of scheduling parameter vector.

$$\begin{cases} \Delta x(k+1) = A(\rho)\Delta x(k) + B(\rho)\Delta u(k) \\ \qquad \Delta y(k) = C\Delta x(k) \end{cases} \quad (2)$$

In this study, the scheduling parameter ρ is chosen to be a function of the real-time failed (front-right) propeller speed n and can be obtained by equation (3)

$$\rho(n) = 1 + 3\{1 - (n(t)/100.7)^3\} \quad (3)$$

where ρ varies from 1 to 2 (2–3) when the propeller speed is dropped from 100.7 to 87.7 rad/s (87.7–69.6 rad/s) with $A(\rho = i) = A_i$ for $i = 1, 2, 3$; see Table 3 for reference. Then, the system model between the trimmed conditions can be obtained by linearly interpolating the adjacent LTI models. For example, when the aircraft is operated at a front-right failed propeller speed $n \in [87.7, 100.7]$ rad/s, in this case, the LPV model (2) is between the adjacent LTI models 1 and 2, and system matrix $A(\rho)$ can be calculated based on the adjacent trimmed model matrices A_1 and A_2 as $A(\rho) = A_1 + (\rho - 1)(A_2 - A_1)$ with ρ obtained by equation (3). To handle the equilibrium condition change for trimmed
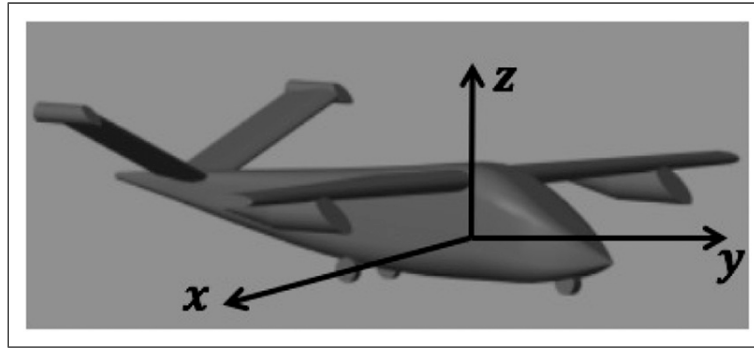
Figure 2. Coordinate definition of urban air mobility aircraft.

Table 3. System input and output definition.

System input	Order	System state	Order
Front right/left propeller acceleration	u_1/u_2	Rigid-body velocity	$x_{1:6}$
Mid right/left propeller acceleration	u_3/u_4	Euler angle	$x_{7:9}$
Rear right/left propeller acceleration	u_5/u_6	Body inertial position	$x_{10:12}$
		Propeller speed	$x_{13:18}$
Lateral speed (V_x)	y_1	Roll angle (θ_y)	y_7
Longitudinal speed (V_y)	y_2	Pitch angle (θ_x)	y_8
Vertical speed (V_z)	y_3	Yaw angle ($-\theta_z$)	y_9
Pitch rate ($\dot{\theta}_x$)	y_4	Lateral displacement (D_x)	y_{10}
Roll rate ($\dot{\theta}_y$)	y_5	Longitudinal displacement (D_y)	y_{11}
Opposite value of yaw rate ($\dot{\theta}_z$)	y_6	Vertical displacement (D_z)	y_{12}

models, equation (2) is extended to the following affine LPV model in equation (4)

$$
\begin{cases}
x(k+1) = x_0(\rho(k+1) + A(\rho(t))(x(k) - x_0(\rho(k))) \\
\qquad\qquad + B(\rho(k))u(k) - (u_0(\rho(k))) \\
y(k) = Cx(k)
\end{cases}
$$

(4)

where Δx, Δu, and Δy in equation (1) are presented in the different form of system states, inputs, and outputs $x(k)$, $u(k)$ and $y(k)$ with its equilibrium conditions x_0 ($\rho(k)$), u_0 ($\rho(k)$), and y_0 ($\rho(k)$). Note that variables x_0 ($\rho(k)$), u_0 ($\rho(k)$), and y_0 ($\rho(k)$) are linearly interpolated equilibrium conditions of the adjacent LTI models following the same method as interpolating the system matrices (see example for $A(\rho)$). It is worth mentioning that $\rho(k+1)$ in equation (4) cannot be directly obtained since it depends on the system response at the next time step. Thus, it is approximated by $\rho(k+1) \approx \rho(k)$, assuming that the equilibrium condition change from the current step to the next is negligible with high sampling rate (one millisecond in this study).

Adaptive MPC controller design of LPV system

This section outlines the adaptive MPC scheme with specific modifications to handle the constraints and time-varying reference in order to reduce computational cost and improving the system performance.

Model predictive control

Letting $\Delta x(k) = x(k) - x_0$ ($\rho(k)$) and $\Delta u(k) = u(k) - u_0$ ($\rho(k)$), state equation (4) can be converted to the following controller design form stated in equation (5)

$$\Delta x(k+1) = A(\rho(k))\Delta x(k) + B(\rho(k))\Delta u(k) \quad (5)$$

Defining $e(k) = \Delta x_{\text{ref}} - \Delta x(k)$ for state tracking purpose, at current time step k, the adaptive MPC controller design[17–19] is to find the constrained control input $\Delta u(k)$ (over the finite horizon) that minimizes the constrained quadratic performance index shown in equation (6) where matrices $Q \geq 0$ and $R > 0$ are control design

$$
\min_{\Delta u(k),\ldots,\Delta u(k+N-1)} \frac{1}{2}\left\{ e^T(k+N)Qe(k+N) + \sum_{m=0}^{N-1}\left[e^T(k+m)Qe(k+m) + \Delta u^T(k+m)R\Delta u(k+m) \right] \right\}
$$

(6)

$$\text{s.t. } G\Delta u(k+m) \leq h, m = 0, \ldots, N-1$$

weighting matrices used to penalize the state error and control, respectively, and G transfers control input Δu to satisfy constraints $h = u_{max} - u_0$ derived based on the actutation saturation u_{max} and current equilibrium condition u_0. At the m-th step of the internal prediction horizon, $e(k + m)$, $\Delta u(k + m)$, and $h(k + m)$ present the predicted tracking error, control input, and its constraints. For a finite prediction horizon of N steps, the predicted quadratic performance index stated in equation (6) can be written in a stage-wise structure in equation (7)

$$\min \frac{1}{2} \left[\hat{e}(k)^T \hat{Q} \hat{e}(k) + \hat{u}(k)^T \hat{R} \hat{u}(k) \right]$$

$$\text{s.t.} \hat{G} \hat{u}(k) \leq \hat{h}(k) \tag{7}$$

where $\hat{e}(k) = \hat{A} e(k) + \hat{B} \hat{u}(k)$, and the transformation matrices from equation (6) to (7) are detailed in equation (8)

other hand, a reasonable selection of tuning parameters and a well-posed optimization problem usually deliver stable closed-loop performance. Benefiting from the linear interpolation of LTI models, the parameter variation of prediction model between each control design step is very small due to continuous system dynamics and small sample period. Thus, in this study, the MPC stability is not guaranteed in theory but demonstrated in simulations. Closed-loop stability will be part of future work.

Motor failure simulation with input constraint variation

Utilizing the constraint handling ability of the MPC, a motor failure simulation structure is introduced in this section. First, power P needed for a propeller spinning at speed n can be calculated by equation (10)

$$\hat{e}(k) = \begin{bmatrix} e(k) \\ e(k+1) \\ \vdots \\ e(k+N) \end{bmatrix}, \Delta \hat{u}(k) = \begin{bmatrix} \Delta u(k) \\ \Delta u(k+1) \\ \vdots \\ \Delta u(k+N-1) \end{bmatrix}, \hat{h} = \begin{bmatrix} h \\ h \\ \vdots \\ h \end{bmatrix}, \hat{R} = \begin{bmatrix} R & 0 & \dots & 0 \\ 0 & R & \dots & 0 \\ \vdots & \vdots & \ddots & \vdots \\ 0 & 0 & \dots & R \end{bmatrix}, \hat{G} = \begin{bmatrix} G & 0 & \dots & 0 \\ 0 & G & \dots & 0 \\ \vdots & \vdots & \ddots & \vdots \\ 0 & 0 & \dots & G \end{bmatrix}$$

$$\hat{Q} = \begin{bmatrix} Q & 0 & \dots & 0 \\ 0 & Q & \dots & 0 \\ \vdots & \vdots & \ddots & \vdots \\ 0 & 0 & \dots & Q \end{bmatrix}, \hat{A} = \begin{bmatrix} I \\ A(\rho) \\ A^2(\rho) \\ \vdots \\ A^N(\rho) \end{bmatrix}, \hat{B} = \begin{bmatrix} 0 & 0 & 0 & \dots & 0 \\ B(\rho) & 0 & 0 & \dots & 0 \\ A(\rho)B(\rho) & B(\rho) & 0 & \dots & 0 \\ \vdots & \vdots & \vdots & \ddots & 0 \\ A^{N-1}(\rho)B(\rho) & A^{N-2}(\rho)B(\rho) & A^{N-3}(\rho)B(\rho) & \dots & B(\rho) \end{bmatrix} \tag{8}$$

As a result, the reformulated optimization problem is stated in equation (9)

$$\min_{\hat{u}} \frac{1}{2} \hat{u}^T(k) \left(\hat{R} + \hat{B}^T \hat{Q} \hat{B} \right) \hat{u}(k) + e^T(k) \hat{A}^T \hat{Q} \hat{B} \hat{u}(k)$$

$$\text{s.t.} \quad \hat{G} \hat{u}(k) \leq \hat{h}(k) \tag{9}$$

where $\hat{u}(k) = [\Delta u^T(k), ..., \Delta u^T(k+N-1)]^T$ is the solved optimization control vector, that is, the optimal solution for the problem defined by equations (5) and (6).

For real-time control at current time step k with a measured or estimated state $\Delta x(k)$, the minimization problem described in equation (9) is solved using quadratic program (QP) solver implemented in Matlab[29] with the solution $\hat{u}(k) = [\Delta u^T(k+0), ..., \Delta u^T(k+N-1)]^T$. Instead of only applying the first control entry at current time step k and repeating the whole optimization process at next time step $k + 1$, a control horizon of N_c is defined, which means that the first N_c control in $\hat{u}(k)$ will be used as the control effort between the current sample time k and sample time $k + N_c - 1$, followed with the new optimization process repeated at time $k + N_c - 1$ to obtain the next control effort $\Delta u (k + N_c : k + 2N_c - 1)$; see Ref. 30 for details.

For MPC of LPV systems, certain closed-loop system stability can be achieved based on the theories developed in Refs. 26, 31, and 32, which could lead to very conservative control law with high computational complexity. On the

$$P = C_p \rho_p n^3 D^5 \tag{10}$$

where C_p, ρ_p, and D denotes the power coefficient, air density, and propeller diameter, respectively. Letting the propeller assembly spin inertia be I_p and the propeller acceleration be $\dot{n}$, the propeller spin dynamics can be formed in equation (11)

$$\dot{n} = \left(-C_p \rho_p D^5 n^2 + T \right) / I_p \tag{11}$$

where T is the propeller motor output torque, and term $-C_p \rho_p D^5 n^2$ calculates the resistant torque at spin speed n. By defining the resistant coefficient $K = C_p \rho_p D^5 / I_p$ and the equivalent motor driven acceleration $u = T/I_p$, the propeller spin dynamics can be expressed in equation (12) due to (11)

$$\dot{n} = -Kn^2 + u \tag{12}$$

The simulation structure for propeller motor failure is shown in Figure 3.

Assuming that the aircraft starts under the normal hovering condition, the motor failure occurs with a sudden torque drop, causing a gradual propeller speed reduction due to the fact that the motor cannot provide the desired torque to maintain the target propeller speed. Meanwhile, since the failed propeller speed is used to calculate the
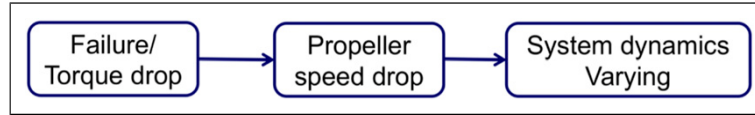
Figure 3. Motor failure simulation.

scheduling parameter of LPV model, the system model parameters will be changed relatively. For example, considering with a failed motor that can only provide $r(t)\%$ of power with respected to the power used under normal hovering condition, the maximum propeller driven torque T_{max} can be calculated based on equation (13)

$$T_{max} = (P_h \times r(t)\%)/n(t) \qquad (13)$$

where P_h is the motor power at hovering. After converting equation (13) to the same unit of control input (dividing the equation by the propeller–motor–rotor assembly inertia I_p), equation (14) presents the real-time MPC control constraint, where $u_{max} = T_{max}/I_p$ can be considered as the equivalent propeller acceleration resulted by the motor torque

$$u_{max} = (P_h \times r(t)\%)/I_p n(t) \qquad (14)$$

After motor failure occurs under hovering condition, the propeller acceleration $\dot{n}(t)$ becomes negative based on equation (12) due to $u < Kn^2(t)$. In summary, the control input constraints $u_{max} = f(n, r)$ for MPC design need to be updated in real-time as a function of propeller speed $n(t)$ and available power percentage $r(t)$.

Dynamic reference compensation

To hold the vehicle at hovering condition, every output reference is set to 0, which means that the control target is to hold the system at its hovering equilibrium condition. It was found, during calibrating the adaptive MPC controller, that even though large penalization was used in the weighting matrix on certain system outputs (including linear speeds and angular positions), these outputs have very slow responses, resulting in large control errors; and sometimes, the closed-loop system is not even stable. In theory, using a sufficient long prediction horizon will lead to an MPC design with improved performance. However, the computational cost will be too large to be practical for real-time implementation.

To achieve desired system performance with feasible computational cost, the dynamic reference compensation method was developed with details explained below. Note that since only incremental propeller acceleration is controlled directly through Δu generated by the adaptive MPC, the propeller speed (or propeller thrust) responses are slow since a significant part of control u is contributed by u_0 that has nothing to do with the MPC controller. To stabilize the hovering operation, the angular speeds (such as pitch, roll, and yaw rates) are directly affected by the propeller thrusts. As for the longitudinal and lateral speeds, in the hovering case without any tilting operation, it can be controlled by manipulating the flight pitch and

roll angles to change the direction of total thrust vector formed by all propellers. On the other side, the flight angular position control can be achieved by setting the reference angular speed based on the feedback angular positions with calibratable negative gains. Last but not the least, vertical drop under motor failure is always critical for hovering control, and it shall be recovered and stabilized by modifying the reference vertical speed correspondingly.

In summary, instead of finding well-calibrated weighting matrices with relative long prediction horizon, the output weighting matrix used in the adaptive MPC control design for flight hovering control is selected to mainly focus on the angular and vertical speeds that are directly affected by the control inputs. As a result, reference angular/vertical speeds are compensated as below in equation (15)

$$\begin{bmatrix} \Delta x_3^{ref} \\ \Delta x_4^{ref} \\ \Delta x_5^{ref} \\ \Delta x_6^{ref} \end{bmatrix} = \begin{bmatrix} 0 & 0 & 0 & 0 & 0 & a_{16} \\ 0 & a_{22} & 0 & a_{24} & 0 & 0 \\ a_{31} & 0 & a_{33} & 0 & 0 & 0 \\ 0 & 0 & 0 & 0 & a_{45} & 0 \end{bmatrix} \begin{bmatrix} \Delta x_1 \\ \Delta x_2 \\ \Delta x_7 \\ \Delta x_8 \\ \Delta x_9 \\ \Delta x_{12} \end{bmatrix} \qquad (15)$$

where Δx_i (i = 1, 2, 7, 8, 9, 12) and Δx_j^{ref} (j = 3, 4, 5, 6) denotes system states and their reference signals with their definitions stated in Table 3. Observed from the simulation results during the controller development, the smoothness of the system response is not satisfactory after adding this compensation. Thus, constraints have been placed on Δx and Δx^{ref} in equation (15), with the calculated reference signal Δx^{ref} filtered using a low-pass first-order filter $H(s)$ stated in Table 4, which improves the MPC control performance significantly with a stable flight.

Framework of adaptive LPV-MPC

The closed-loop system framework is shown in Figure 4, where Δx and Δu are the controlled states and inputs equivalent to $\Delta x(k)$ and $\Delta u(t)$ stated in equation (2). Based on the real-time reference signal x^{ref} and the system state feedback signal Δx, the MPC control generates the optimized state feedback control effort Δu that will be combined with $u_0(\rho)$ (current control equilibrium) to form system control signal $u = \Delta u + u_0(\rho)$, where ρ is calculated scheduling parameter based on the front-right propeller speed $n(t)$ (see equation (3)). The system model presents the nonlinear flight dynamics with system output y. In this study, all the system states are assumed to be measurable due to available sensor set for the aircraft

Table 4. Adaptive MPC controller spec parameters.

Parameter	Value	Parameter	Value
$Q_{[1,1]}$	1	$Q_{[2,2]}$	1
$Q_{[3,3]}$	1000^2	$Q_{[4,4]}$	20000^2
$Q_{[5,5]}$	20000^2	$Q_{[6,6]}$	1000^2
$R_{[1:6,1:6]}$	$0.1^2 \times I_6$	Step size	1 ms
Prediction horizon	20 steps	Control horizon	4 steps
min $\Delta u_{[1:6]}$	$-Kn^2_{[1:6]}(t)$	Max $\Delta u_{[1:6]}$	$-Kn^2_{[1:6]}(t)+\max u_{[1:6]}$
a_{16}	-0.3	a_{22}	0.1
a_{24}	-1.5	a_{31}	-0.1
a_{33}	-1.5	a_{45}	-1
s.t $\Delta x_{[1,2]}$	$[-5, 5]$	s.t $\Delta x_{[7,8]}$	$[-0.5, 0.5]$
s.t $\Delta x^{ref}_{[4,5,6]}$	$[-0.03.0.03]$	$H(s)$	$1/0.2s + 1$
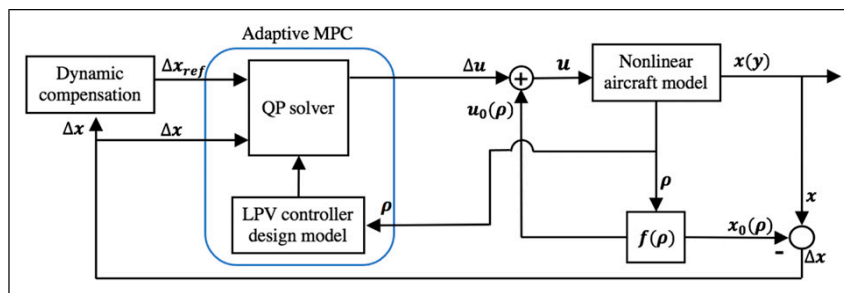
Figure 4. Structure of adaptive model predictive control controller.

as $y = x$. And the state feedback signal Δx is calculated as $\Delta x = x - x_0(\rho)$, which completes the closed-loop flight control system.

Simulation Results and Discussions

The control design parameters are carefully calibrated based on the rigid-body aircraft model response with the simulation structure shown in Figure 4, and the detailed control design parameters are listed in Table 4, where these design parameters are defined in equations (6) and (15). The simulation study was conducted using MATLAB 2019b running on a MacBook Pro equipped with a 2.2 GHz Intel Core i7 processor, and the run-time for a 20-s flight simulation with both adaptive MPC strategy and nonlinear aircraft model is about 12 s, which is considered acceptable for real-time implementation since simulation time is shorter than actual time even with nonlinear aircraft model included in the simulation.

First, we assumed that the available front-right motor power failed from 100% to 33.3% (models 1 to 3 in Table 2) with stable hovering as the initial aircraft condition. For comparing the system responses between LPV and nonlinear rigid-body models, the designed adaptive MPC controller was used to conduct closed-loop simulations based on both nonlinear rigid-body and LPV models, respectively, where the simulation results are denoted by rigid-body model and LPV model in Figure 5, respectively. In this ideal failure situation, the rear-left (#6 in Figure 1) propeller speed is synchronized with the failed front right (FR) (#1 in Figure 1) one and the rest four healthy propellers are operating at the same speed higher than their normal hovering speeds to compensate the thrust lost due to speed reduction of front-right (#1 in Figure 1) and rear-left (#6 in Figure 1) propellers. Benefiting from these symmetric propeller responses, the oscillation dynamics only appears for the vertical speed; see Figure 5 for the vertical speed and acceleration.

In both cases, the aircraft vertical speed V_z and its acceleration $\dot{V}_z$ converge to stable condition in 5 s with a magnitude of speed oscillation less than 0.13 m/s. Small response difference can be observed at the beginning of simulation as the maximum vertical speed drop from the rigid-body model is slightly larger (-0.127 m/s) than that of LPV one (-0.119 m/s). For the rest of studies in this article, the simulations are based on the closed-loop system performance of nonlinear rigid-body aircraft model to make the simulation results practical.

In practice, it is necessary to further study the control performance under certain non-zero condition since the aircraft could operate under non-equilibrium condition at the same time when motor failure happens. The scenario that UAM vehicle experience a sharp gust disturbance is considered in this study. The gust disturbance is assumed to generate a sudden pitch rate $\dot{\theta}_x = -2.9$ deg/s, leading to the vehicle nose dipping at the beginning (0 s) of simulation. Three cases are studied in this section, assuming
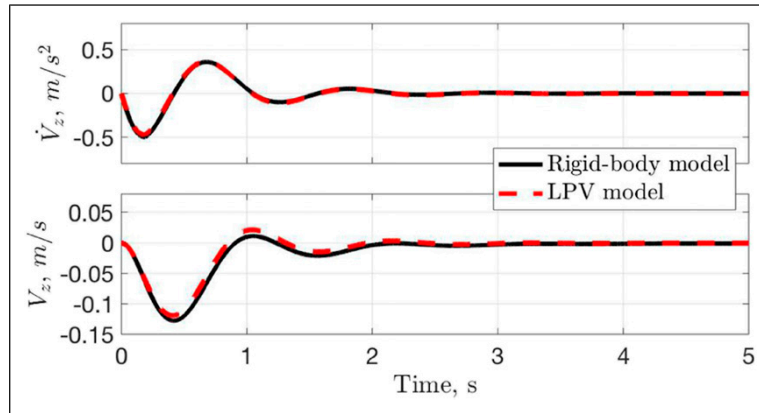
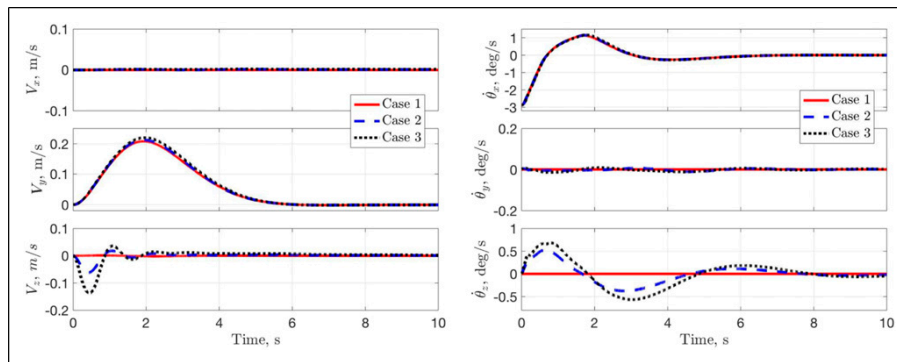**Figure 5.** Vertical speed and acceleration of ideal failure case.

Figure 6. Flight rigid-body velocity of propeller #1 failure situations.

that the flight is under normally hovering initially, with front-right motor (#1) operating under healthy condition (100%), partially failed condition 66%, or 33% of normal hovering power, denoted as Cases 1, 2 and 3, respectively. The vehicle rigid-body velocity is shown in Figure 6.

With an initial pitching rate of $\dot{\theta}_x = -2.9$ deg/s shown in top-right plot of Figure 6, the vehicle moves forward at the very beginning with a maximum longitudinal speed V_y of 0.208, 0.213, and 0.22 m/s for Cases 1, 2, and 3, respectively. Also, all three cases have very similar responses for V_x, $\dot{\theta}_x$, and $\dot{\theta}_y$ under different available power for motor #1. As for vertical speed V_z, the oscillation magnitude is increased as case number increases from 1 to 3 due to rising motor failure severity. Last but not the least, it can be observed that the oscillation magnitude $\dot{\theta}_z$ also goes up as case number increases from 1 to 3 with no oscillation for Case 1. This motion is mainly affected by the unbalanced air drag from propellers, which can be eliminated with symmetric propeller control actuation (see Case 1). However, under motor failure situations (Cases 2 and 3), unsymmetric control could happen since the six motors are operated under different available power levels.

In order to further understand and compare the vehicle behaviors, propeller speeds of Cases 1 and 3 are shown in

the left plot of Figure 8, where different colors present the propeller locations (e.g., FR: front right) with solid and dotted lines denoting Cases 1 and 3, respectively. Recall the initial pitching-down motion caused by simulated gust disturbance, the motion of controlled propellers can be explained intuitively. In general, the vehicle requires a pitch-up acceleration to recover from the initial pitching-down motion, which can be achieved by increasing the thrusts generated from front propellers and reducing rear thrust. This is validated by the propeller speed responses of Case 1 (solid line). However, due to the limited front-right motor power in Case 3, the front-right (#1) motor cannot provide enough thrust to balance the vehicle, leading to increasing middle two propeller efforts (MR: #3 and ML: #4). As the failure gets severe, except the failed front-right propeller and its central symmetry one (RL: #6), all other propeller speeds increases correspondingly, with the highest speed for the front-left (FL: #2) one. Last, the failed front-right propeller speed is slightly varying between 3 and 6 s to balance the vehicle yaw motion, indicating the significance of coordinated control even under failed condition. In summary, the adaptive MPC controller is able to stabilize the vehicle in 10 s for all three failure cases.

Noting that the failure study for propeller #1, #2, #5, or #6 is the same since their locations are symmetric; see

Figure 1. However, to validate the overall control performance with all possible single motor failure, the failure study of propeller #3 or #4 becomes necessary since its failure is different from that of propeller #1. As a result, propeller #4 is selected for failure study with the equilibrium conditions same as propeller #1 at 100% and 33% available power of normal hovering condition. The same adaptive MPC (see Table 4 for control design parameters), used in the propeller #1 failure study, is used for propeller #4 failure study, where 33% is the available power for the failed #4 motor with initial conditions $\dot{\theta}_x = -2.9$ deg/s,

$\dot{\theta}_x = -4.64$ deg/s, and $\dot{\theta} = -2.9\dot{\theta}_x + -2.9\dot{\theta}_y$ deg/s for Cases 4, 5, and 6, respectively.

The rigid-body velocities are shown in Figure 7. In general, the trends and characteristics of responses are similar to Cases 1, 2, and 3. It is worth mentioning that for Cases 4 and 5 with initial pitch motion, the oscillations of roll and yaw angles are eliminated compared with Cases 2 and 3, which benefits from the symmetric responses of left and right propellers. Propeller speeds are also shown in the right plot of Figure 8, where the highest speed occurs at the front-left propeller that generates the most efficient thrust
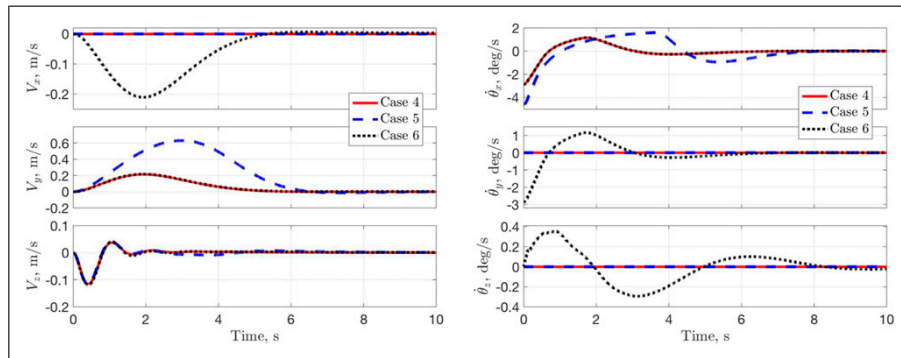

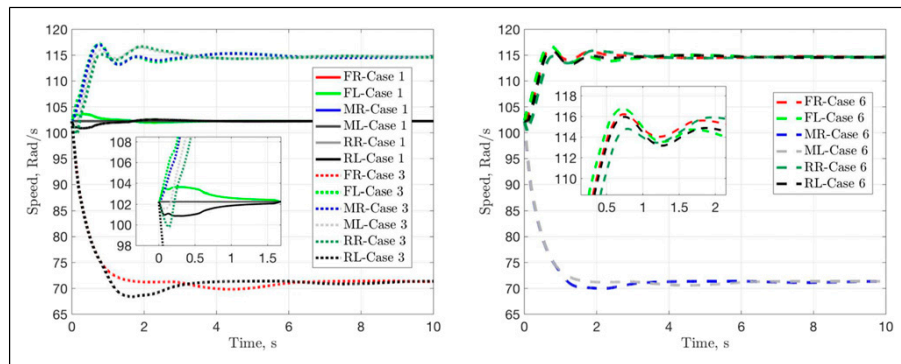**Figure 7.** Flight rigid-body velocity of propeller #4 failure situations.

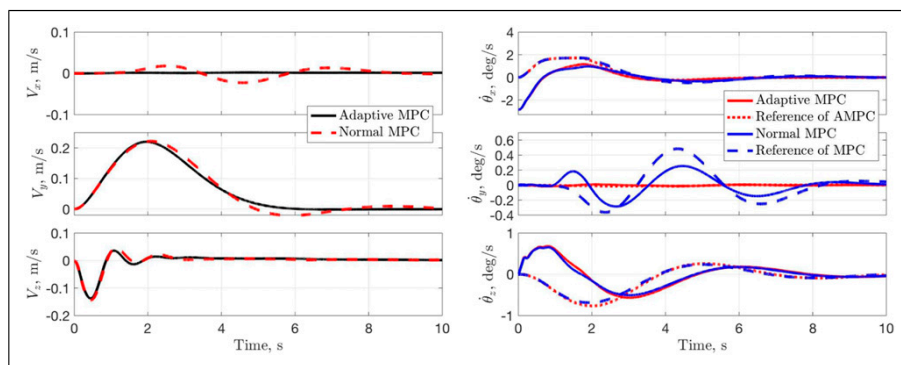**Figure 8.** Speed of propellers of Case #1#3 (left) and #6 (right).

Figure 9. Rigid-body velocity comparison of AMPC and MPC.
Note: AMPC: adaptive model predictive control; MPC: model predictive control.

for recovering the joint motion of the initial pitch and roll disturbance.

In order to validate the capability of proposed adaptive MPC, a normal MPC was designed and its design weighting is optimized based on the model with healthy motors (system at $\rho = 1$) with the same reference dynamic compensation and motor failure constraints as these for Case 3. Note that u_0 in the comparison simulations is the same and scheduled by ρ calculated from failed propeller speed n, but Δu is different since Δu from the conventional MPC is designed based on the LTI system at $\rho = 1$ and Δu from the adaptive MPC is based on the LPV model with ρ varying from 1 to 3. Assuming that both failure situations are the same as Case 3, that is, the initial pitching speed is $\dot\theta_x = -2.9$ deg/s with 33% of normal hovering power available for the front-right (FR #1) motor, the rigid-body velocities are shown in Figure 9.

Figure 10. Speed of propellers comparison of AMPC and MPC. Note: MPC: model predictive control.

It is obvious that flight speed oscillations are smaller in all x, y, and z directions under adaptive MPC. The angular speeds are shown in the right plot of Figure 9 with the related reference signal also plotted in dotted- and dashed-lines for adaptive and normal MPC, respectively. The angular speeds approach their reference signals under both control strategies, and reference signals are also gradually converging to zero. The most significant difference is shown in pitch rate $\dot\theta_y$, where relatively large oscillation can be observed for the conventional MPC. This is due to the fast initial propeller failure response, as variation control signal $u = u_0 + \Delta u$ is dominated by u_0, leading to very similar responses in both cases. However, after 0.9 s, variation of u_0 becomes small and Δu dominates the control gradually. In the conventional MPC, the system model used in control design is not able to capture the aircraft dynamics variation caused by the failure but adaptive MPC does, which leads to the larger oscillation in $\dot\theta_y$.

The propeller speed responses are also shown in Figure 10. It can be observed that the speed trajectories of failed front-right (FR: #1) propeller and symmetric rear-left (RL: #6) one are the same for both cases at the beginning since it is a natural process due to insufficient propeller driven torques. As for the other four propellers, the magnified region shows the start of propeller speeds deviations between adaptive and conventional MPC, since Δu takes over the control as discussed above, leading to different recovering responses. Especially the adaptive MPC strategy leads to a much smaller roll rate oscillation.

In summary, the designed adaptive MPC is able to stabilize the aircraft under possible propeller failure cases with different failure percentages, propeller locations, and initial disturbances. Also, the adaptive MPC improves the closed-loop system performance since the LPV model used for MPC design varies based on the real-time flight condition, which reduces the modeling error between the control design model and the actual physical system. Last,
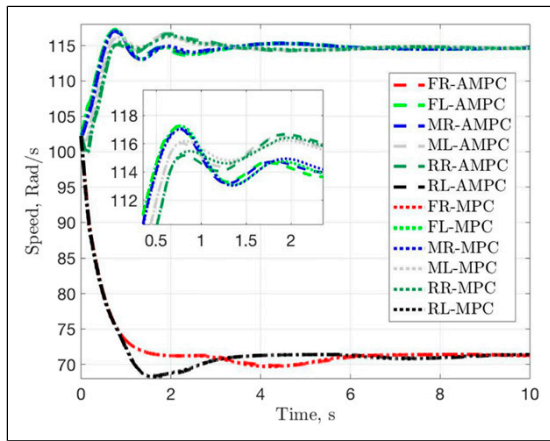
Table 5. RMSE of simulation results.

Case	#1	#2	#3 (AMPC)	#3 (MPC)	#4	#5	#6
Failed propeller	N/A	FR	FR	FR	ML	ML	ML
Available power	N/A	66%	33%	33%	33%	33%	33%
Direction of disturbance	$\dot\theta_x$	$\dot\theta_x$	$\dot\theta_x$	$\dot\theta_x$	$\dot\theta_x$	$\dot\theta_x$	$\dot\theta_x$ and $\dot\theta_y$
Magnitude of disturbance (deg/s)	−2.9	−2.9	−2.9	−2.9	−2.9	−4.64	−2.9 and −2.9
Peak power rotor position	FL/FR	FL	FL	FL	FL/FR	FR/RL	FL
Peak motor power (%)	108.9%	131.4%	158.1%	158.1%	154.0%	154.4%	156.0%
V_x	0	0.0010	0.0015	0.0108	0	0	0.0917
V_y	0.0913	0.0933	0.0968	0.1003	0.0937	0.3170	0.0952
V_z	0	0.0124	0.0283	0.0301	0.0228	0.0233	0.0237
$\dot\theta_x$	0.5800	0.5870	0.5962	0.5814	0.5873	1.0650	0.5902
$\dot\theta_y$	0	0.0044	0.0063	0.1308	0	0	0.5903
$\dot\theta_z$	0	0.2031	0.3041	0.2791	0	0	0.1609
Sum	0.6720	0.9013	1.0333	1.1325	0.7038	1.4054	1.5520

Note: RMSE: root mean square error; FR: front right; MPC: model predictive control.

the root mean square error (RMSE) of all studied cases are summarized in Table 5 with zero references.

Conclusion

This article applies the adaptive MPC scheme to hovering control under propeller motor failure for a six-rotor eVTOL UAM vehicle. The nonlinear rigid-body vehicle system model, developed earlier, is linearized under different failed propeller speeds for a given motor failure percentage to generate a set of LTI models for MPC design. A LPV model is developed based on the set of obtained LTI models and used for adaptive MPC strategy. The time-varying power constraints of propeller motors are considered in control design, and dynamic reference compensation is also used to improve the vehicle recovery performance with reduced computational cost. The simulation results show that the designed adaptive MPC controller is able to stabilize the vehicle under all single motor failure cases, and the overall RMSE of the vehicle rigid-body velocity oscillations can be significantly reduced using the adaptive MPC by 8.77% compared with conventional MPC. The future work is to study the vehicle tilting transition control using the adaptive LPV–MPC framework.

ORCID iD

Guoming Zhu ⓘ https://orcid.org/0000-0002-2101-2698

References

1. Binder R, Garrow L, German B, et al. "If you fly it, will commuters come? Predicting demand for evtol urban air trips." In: AIAA conference, Atlanta, Georgia, 25–29 June 2018, pp. 1–41.

2. Dorrington GE. "Performance of electric vertical take-off and landing (EVTOL) hovering craft," In: AIAC18: 18th Australian international aerospace congress HUMS-11th defence science and technology (DST) international conference on health and usage monitoring (HUMS 2019): ISSFD-27th international symposium on space flight dynamics (ISSFD), engineers Australia, Melbourne, Australia, 1 January 2019. Royal Aeronautical Society, 2019, p. 84.

3. Kleinbekman IC, Mitici MA and Wei P, "eVTOL arrival sequencing and scheduling for on-demand urban air mobility." In: 2018 IEEE/AIAA 37th digital avionics systems conference (DASC), London, UK, 23–27 September 2018. IEEE, 2018, pp. 1–7.

4. German B, Daskilewicz M, Hamilton TK, et al. "Cargo delivery in by passenger eVTOL aircraft: a case study in the San Francisco Bay Area," In: 2018 AIAA aerospace sciences meeting, Kissimmee, FL, 8–12 January 2018, p. 2006.

5. Pradeep P and Wei P. "Heuristic approach for arrival sequencing and scheduling for eVTOL aircraft in on-demand urban air mobility," In: 2018 IEEE/AIAA 37th digital avionics systems conference (DASC), London, UK, 23–27 September 2018. IEEE, 2018, pp. 1–7.

6. Skuhersky M, "A first-principle power and energy model for eVTOL vehicles." PhD thesis, Melbourne, FL: Florida Institute of Technology, 2019.

7. Pradeep P and Wei P. "Energy efficient arrival with RTA constraint for urban eVTOL operations." *2018 AIAA Aerosp Sci Meet*. 2018; 16: 2008.

8. Daskilewicz M, German B, Warren M, et al. "Progress in vertiport placement and estimating aircraft range requirements for eVTOL daily commuting." In: 2018 aviation technology, integration, and operations conference, Atlanta, GA, 25–29 June 2018, p. 2884.

9. Payuhavorakulchai P. "*Cost analysis of EVTOL configuration design for air ambulance in Japan*." Tokyo, Japan: Keio University, 2019.

10. Vegh JM, Botero E, Clarke M, et al. "Current capabilities and challenges of NDARC and SUAVE for eVTOL aircraft design and analysis." In: AIAA propulsion and energy 2019 forum, Indianapolis, IN, 19–22 August 2019, p. 4505.

11. Boddupalli S-S. "Estimating demand for an electric vertical landing and takeoff (eVTOL) air taxi service using discrete choice modeling," PhD thesis, Atlanta, GA: Georgia Institute of Technology, 2019.

12. Lombaerts T, Kaneshige J, Schuet S, et al. "Nonlinear dynamic inversion based attitude control for a hovering quad tiltrotor eVTOL vehicle." In: AIAA scitech 2019 forum, San Diego, CA, 7–11 January 2019, p. 0134.

13. Basset P-M, Vu BD, Beaumier P, et al. "*Models and methods at ONERA for the presizing of eVTOL hybrid aircraft including analysis of failure scenarios*." Phoenix, AZ: AHS Forum, 2018.

14. Tashreef S, Iftekhar L and Azmeen-ur Rahman S. "Design of a crash-resistant PD-controlled quadcopter using coaxial propeller system." In: 2016 international conference on unmanned aircraft systems (ICUAS), Arlington, VA, 7–10 June 2016. IEEE, 2016, pp. 986–992.

15. Saied M, Shraim H, Francis C, et al. "Controllability analysis and motors failures symmetry in a coaxial octorotor," In: 2015 third international conference on technological advances in electrical, electronics and computer engineering (TAEECE), Beirut, Lebanon, 29 April–1 May 2015, IEEE, 2015, pp. 245–250.

16. Avant T, Lee U, Katona B., et al. "Dynamics, Hover Configurations, and Rotor Failure Restabilization of a Morphing Quadrotor." In: 2018 annual American control conference (ACC), Milwaukee, WI, 27–29 June 2018, IEEE, 2018, pp. 4855–4862.

17. Camacho EF and Alba CB. *Model Predictive Control*. Secaucus, NJ: Springer Science & Business Media, 2013.

18. Mayne DQ, Rawlings JB, Rao CV, et al.. "Constrained model predictive control: stability and optimality," *Automatica* 2000; 36(6): 789–814.

19. Garcia CE, Prett DM and Morari M. "Model predictive control: theory and practice—a survey." *Automatica* 1989; 25(3): 335–348.

20. Fukushima H, Kim T-H and Sugie T. "Adaptive model predictive control for a class of constrained linear systems based on the comparison model." *Automatica* 2007; 43(2): 301–308.

21. Kim J-S. "Recent advances in adaptive MPC." In: ICCAS 2010, Gyeonggi-do, Korea, 27–30 October 2010. IEEE, 2010. 218–222.

22. Shamma JS. "An overview of LPV systems." *Control of Linear Parameter Varying Systems with Applications*. Secaucus, NJ: Springer, 2012, pp. 3–26.

23. Qu S, He T and Zhu GG. "Engine EGR valve modeling and switched LPV control considering nonlinear dry friction," *IEEE/ASME Transactions on Mechatronics* 2020; 25: 1668–1678.

24. Qu S, He T and Zhu GG. "LPV modeling and switched control for EGR valves with dry friction." In: 2019 IEEE conference on control technology and applications (CCTA), Hong Kong, China, 19–21 August 2019. IEEE, 2019, pp. 400–405.

25. Ding B, "Dynamic output feedback MPC for LPV systems via near-optimal solutions." In: Proceedings of the 30th Chinese control conference, Yantai, China, 22–24 July 2011. IEEE, 2011, pp. 3340–3345.

26. Casavola A, Famularo D and Franze G. "A feedback min-max MPC algorithm for LPV systems subject to bounded rates of change of parameters." *IEEE Trans Automatic Control* 2002; 47(7): 1147–1153.

27. Su W, Qu S, Zhu GG, et al. "A control-oriented dynamic model of tiltrotor aircraft for urban air mobility." In: AIAA scitech forum, virtual event, 11–15 January 2021. pp. 0091.

28. Al-Jiboory AK, Zhu G, Swei SS-M, et al. "LPV modeling of a flexible wing aircraft using modal alignment and adaptive gridding methods." *Aerospace Sci Technol* 2017; 66: 92–102.

29. Schmid C and Biegler LT. "Quadratic programming methods for reduced hessian SQP." *Comput Chem Eng* 1994; 18(9): 817–832.

30. Phuong TH, Belov MP and Van Thuy D. "Adaptive model predictive control for nonlinear elastic electrical transmission servo drives." In: 2019 IEEE conference of Russian young researchers in electrical and electronic engineering (EIConRus), Saint Petersburg and Moscow, Russia, 28–31 January 2019, IEEE, 2019, pp. 704–708.

31. Kothare MV, Balakrishnan V and Morar M. "Robust constrained model predictive control using linear matrix inequalities." *Automatica* 1996; 32(10): 1361–1379.

32. Boyd S, El Ghaoui L, Feron E, et al. *Linear matrix inequalities in system and control theory*. Philadelphia, PA: SIAM, 1994.